Spin-glass like behaviour in the nanoporous Fe_2O_3 with amorphous structure

2008 J. Phys.: Condens. Matter 20 295228

(http://iopscience.iop.org/0953-8984/20/29/295228)

J. Phys.: Condens. Matter **20** (2008) 295228 (7pp) doi:10.1088/0953-8984/20/29/295228

Spin-glass like behaviour in the nanoporous Fe_2O_3 with amorphous structure

M Thakur[1], S Majumdar[1], S Giri[1], A Bhaumik[2], M Nandi[2], H Nakamura[3,4], H Kobayashi[3] and T Kohara[3]

[1] Department of Solid State Physics and Center for Advanced Materials, Indian Association for the Cultivation of Science, Jadavpur, Kolkata 700 032, India
[2] Department of Materials Science and Center for Advanced Materials, Indian Association for the Cultivation of Science, Jadavpur, Kolkata 700 032, India
[3] Graduate School of Material Science, University of Hyogo, Kamigori, Ako-gun, Hyogo 678-1297, Japan

E-mail: sspsg2@iacs.res.in (S Giri)

Received 23 April 2008, in final form 16 June 2008
Published 1 July 2008
Online at stacks.iop.org/JPhysCM/20/295228

Abstract

The porous Fe_2O_3 was synthesized chemically. The average size of the particle was ~85.0 nm, which was observed by scanning electron microscopy. The signature of porous structure was confirmed by a N_2 adsorption/desorption isotherm and intense x-ray powder diffraction peak at low angle. The x-ray diffraction pattern at high angle indicates the amorphous structure. Mössbauer investigations show that the value of the hyperfine field is ~498.0 kOe at 4.2 K which is much smaller than that of the hyperfine field of crystalline α/γ-Fe_2O_3 and consistent with the values of amorphous Fe_2O_3. The temperature dependence of zero-field cooled magnetization exhibits a peak at 18.0 K (T_f), where T_f follows the Almeida–Thouless relation as $T_f \propto H^{2/3}$. The ageing phenomenon of the magnetic relaxation below T_f and the memory effect in the field-cooled magnetization indicate the typical features of the classical spin-glass compounds below the spin freezing temperature at T_f.

(Some figures in this article are in colour only in the electronic version)

1. Introduction

Porous magnets are currently at the forefront of molecular materials research because the coexistence of magnetic and porous properties opens a new perspective for the development of low-density magnetic materials, magnetic sensors, and multifunctional materials [1]. The porous structure of the magnet creates a large fraction of the surface to volume ratio. The magnetism near the surface of a magnetically ordered solid differs significantly from the bulk properties, due to several factors such as reduced symmetry, lack of coordination numbers, and disorder from defects or strains on the large surface area [2]. The existence of a large surface area can also affect the magnetic properties in the interior of the material, such as the magnetic domain structure and spin arrangements. Such effects may extend from the surface into the interior from the order of a few tens to more than several thousands of angstroms. One of the fundamental problems of surface magnetism is, therefore, to determine the ground-state involved with the surface effect.

In this study, we are interested in the surface enhanced effect on the magnetic properties of porous nanomagnets. The porous Fe_2O_3 is prepared here by the classical surfactant templating method, which typically exhibits an amorphous structure for the oxide compounds [3, 4]. Herein, we also observe the amorphous structure of porous Fe_2O_3 with average particle size ~85.0 nm. Recently, extensive investigations on amorphous Fe_2O_3 suggest the feature of a spin-cluster state below the spin freezing temperature [5, 6]. Akamatsu *et al* reported the typical features of spin-glass (SG) behaviour in dilute Fe_2O_3–TeO_2 glass with an amorphous structure [7].

[4] Present address: Department of Materials Science and Engineering, Kyoto University, Kyoto 606-8501, Japan.

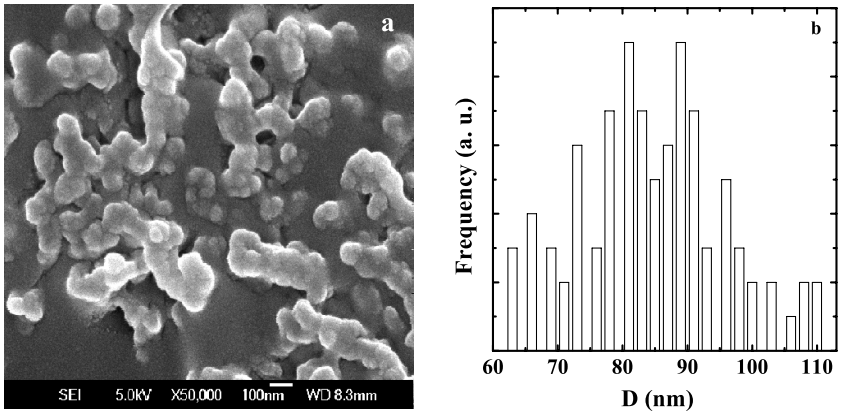

Figure 1. (a) SEM image (scale given in the figure is 100 nm); (b) histogram of the particle size for 'free powder'.

In this paper, we report on porous Fe_2O_3 exhibiting an amorphous structure in another unique system, which also reveals the typical feature of classical SG compounds from the static and dynamic features dc magnetization study.

2. Experimental procedure

Porous iron oxide was synthesized hydrothermally at 348.0 K using self-assembly of surfactant micelles as a structure directing agent (SDA) [3]. Stearic acid (SA) was used as template for the synthesis of porous iron oxide. Oxalic acid (OA) was used as a complexing agent and ferric chloride was used as the Fe(III) source. In the course of synthesis of the material 1.63 g of $FeCl_3$ (0.01 mol) was dissolved in an aqueous solution of OA (0.058 g of OA in 10 g of H_2O) under vigorous stirring at room temperature for 10 min. Then a premixed solution of SA (1.42 g, 0.005 mol) in 10 ml ethanol was added drop wise to the mixture under continuous stirring for 0.5 h. After 2 h of continuous stirring tetramethylammonium hydroxide (TMAOH, 25% aqueous, Aldrich) was added dropwise into the mixture and the pH was maintained at ca 11.0. The resulting mixture was stirred for another 4 h at room temperature and then thermally treated at 348.0 K for 72 h under static conditions. The brown solid was recovered by filtration, washed several times with water, and dried under vacuum. The as-synthesized Fe_2O_3–SDA composite was extracted thrice with ethanolic NaOH solution to remove the stearic acid and molecules for generating porosity. Note that the pH of the solution and optimal thermal treatment temperature was crucial to obtain the maximum surface area and best porous structure exhibiting maximum peak intensity in the low angle x-ray diffraction pattern. When the thermal treatment temperature was below 348 K, a disordered porous structure was observed with much lower peak intensity in the low angle x-ray diffraction. We also note that at high temperature SA cannot act as a structure directing agent, because it cannot form stable micelles.

We used low and high angle x-ray powder diffraction (Seifert XRD 3000P) using a Cu Kα radiation to confirm the signature of pores and the structural properties. Scanning electron microscopy (SEM) JEOL JSM-6700F was also used to observe the size and distribution of size of the particles. An Autosorb 1C (Quantachrome) was used to confirm the porosity of the sample and determination of pore size. A thermogravimetric analyzer (TGA) from TA instruments (SDT Q600) was used to characterize the chemical composition. The magnetization study was performed using a commercial superconducting quantum interference device (SQUID) magnetometer of MPMS, 5 T and MPMS, XL (evercool model). In the case of zero-field cooled (ZFC) measurements the sample was cooled down to the desired temperature from well above the transition temperature in a zero magnetic field and measurements were performed in the heating cycle with magnetic field, while for field-cooled (FC) case the sample was cooled in the presence of a magnetic field and measured during heating of the sample as for the ZFC measurement. We measured the magnetization for powdered and fixed samples, where the powdered sample was fixed in a nonmagnetic stycast matrix. Henceforth, we call the powdered and fixed samples 'free powder' and 'fixed powder', respectively. It was difficult to mix the powders homogeneously with the matrix while fixing the sample and a portion of the 'fixed powder' was considered for the magnetization measurements. Therefore, we could not determine the precise mass of the sample in the mixture and the unit of magnetization of the 'fixed powder' is given in arbitrary units. The Mössbauer spectra were recorded in a transmission geometry using a ∼370 MBq ^{57}Co source in a Rh matrix with a Wissel velocity drive unit in a constant acceleration mode. The spectrometer was fitted with a liquid helium cryostat for the measurement at low temperature. The velocity scale is calibrated by α-iron at room temperature.

3. Experimental results

3.1. Chemical characterization and structural properties

The size and shape of the particles observed in the SEM image for the 'free powder' can be seen in figure 1(a), where a wide distribution of the particle size between ∼60 and ∼110 nm is shown in figure 1(b) with an average particle size around ∼85.0 nm. The existence of pores in the sample is confirmed by the studies on N_2 adsorption/desorption isotherms, which

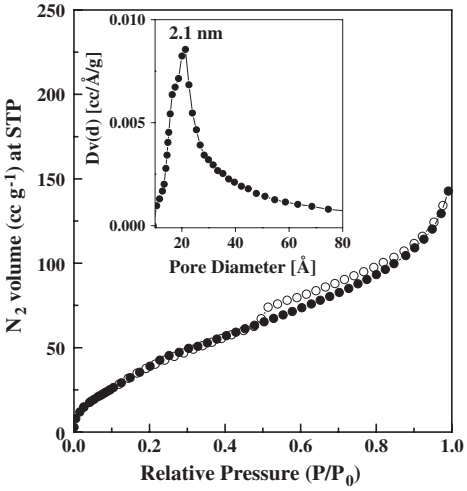

Figure 2. N_2 adsorption/desorption isotherm for the template free porous Fe_2O_3. The inset shows the pore size distribution.

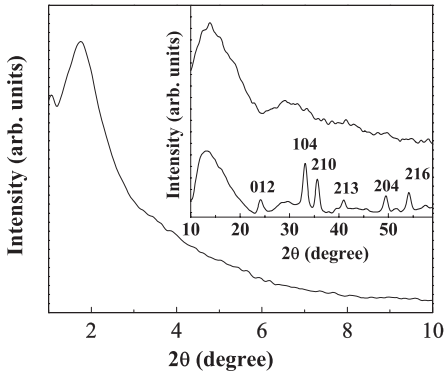

Figure 3. Low angle x-ray diffraction peak of the as-synthesized sample. The absence of the high angle diffraction peak is shown in the inset of the figure for the as-synthesized sample and the diffraction peaks of α-Fe_2O_3 phase for the as-synthesized sample heated at 473.0 K for 4 h.

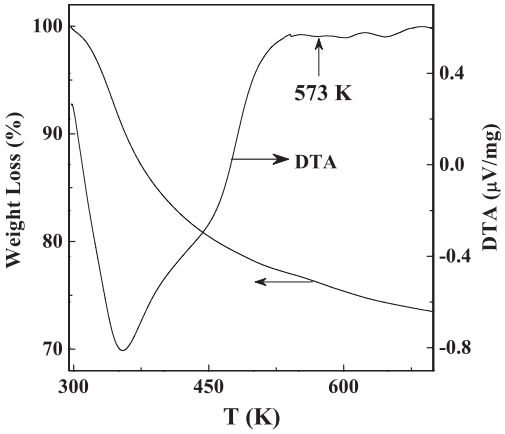

Figure 4. Temperature dependence of percentage of weight loss and differential thermal analysis (DTA) curve for porous iron oxide.

are shown in figure 2. The typical features of an isotherm for porous materials are observed with a significant increase of N_2 volume at standard temperature and pressure (STP) with normalized pressure (P/P_0) in between 0.025 and 0.50, where P_0 is 1 atmospheric pressure. The irreversibility between adsorption and desorption isotherms is observed for $P/P_0 > 0.50$ and is attributed to the porous structure. The BET surface area of porous Fe_2O_3 is 179 $m^2\ g^{-1}$, which agrees well with other porous materials synthesized by a similar surfactant templating method [4]. The average pore size ($\sim$2.1 nm) can be determined from the differential increase of pore volume, which is shown in the inset of figure 2. The signature of pores is further confirmed by the low angle x-ray powder diffraction, which is shown in figure 3. A sharp peak corresponding to the values of diffraction plane, $d = 5.05$ nm is observed at $2\theta = 1.75°$ indicating that the average size of the pores is below 5.05 nm, consistent with the N_2 adsorption/desorption results. We do not observe any diffraction peak at high angle (inset of figure 3) indicating that the porous sample is amorphous in character. The broadened peak around $2\theta \approx 13°$ appearing in the diffraction pattern is ascribed to the glass sample holder. However, the crystalline phase of α-Fe_2O_3 is observed when the sample was heated at 473.0 K for 4 h. The diffraction pattern of α-Fe_2O_3 is shown in the inset of figure 3. In addition, the low angle peak at 1.75° disappeared indicating that the porous structure is destroyed by heating at 473.0 K. We further note that a wide distribution of particle size in between $\sim$100 nm and $\sim$1 μm was observed for crystalline α-Fe_2O_3. In the case of synthesis of materials in aqueous solution the probability of a minor impurity phase of ferrihydrite cannot be ruled out. We did not observe the other impurity phase in the diffraction patterns, but x-ray diffraction cannot determine the impurity phase efficiently below $\sim$2%. The absence of α-FeOOH and $Fe(OH)_3$ was further confirmed by differential thermal analysis (DTA), where the signatures of the above phases are confirmed by the endothermic effect around 573.0 K [8]. Here, we did not observe the endothermic effect around 573 K indicated by the arrow in figure 4. The endothermic effect around 373.0 K is attributed to the evaporation of water, which is commonly adsorbed within the pores for porous materials.

3.2. Magnetization results

The 'free powder' and 'fixed powder' with porous structure were considered in the magnetization studies. The temperature dependence of ZFC–FC magnetization measured at 50.0 Oe is shown in figure 5 for 'free powder', where a peak is observed at 18.0 K (T_f) in the ZFC magnetization. The linear plot of inverse susceptibility (H/M) measured at magnetic field, $H = 50$ Oe against temperature is shown in the inset of figure 5. The value of the paramagnetic moment is estimated to be $\mu_{eff} \approx 2.70\ \mu_B$ with a paramagnetic Curie–Weiss temperature, $\Theta_c \approx -4.5$ K, which is obtained from the linear plot of the temperature dependence of H/M. The value of μ_{eff} is much smaller than that of the high spin Fe^{3+} ($\mu_{cal} = 5.92$). Note that the small value of μ_{eff} ($\sim$3.0 μ_B) was also reported for amorphous Fe_2O_3 [9]. We observed ambiguous results when the measurements were performed at higher fields, where the magnitude of susceptibility (M/H) changes significantly

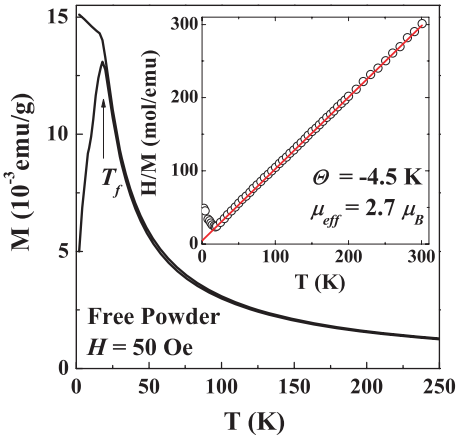

Figure 5. Temperature dependence of zero-field cooled (ZFC) and field-cooled magnetization for the 'free powder'. The peak at $T_f = 18.0$ K in the ZFC magnetization is indicated by the arrow. The inset exhibits the Curie–Weiss behaviour of the inverse susceptibility measured at 50.0 Oe.

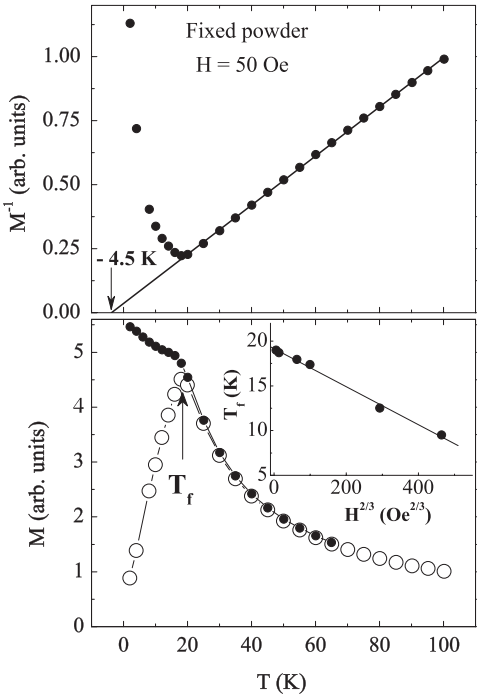

Figure 6. (Top panel) Inverse of the zero-field cooled (ZFC) magnetization against temperature measured at 50.0 Oe for the 'fixed powder'. The solid straight line indicates the Curie–Weiss behaviour. (Bottom panel) Temperature dependence of ZFC and field-cooled (FC) magnetization with a peak at $T_f = 18.0$ K in ZFC magnetization. The magnetic field dependence of T_f following the Almeida–Thouless relation is shown in the inset of the figure.

even in the paramagnetic state at different measured fields ($H > 50.0$ Oe).

In order to find out the origin of such ambiguity the temperature dependence of magnetization for the 'fixed powder' was measured at different fields, which do not show any change in the magnitude of H/M in the paramagnetic state. An example of the inverse of magnetization plotted against temperature is shown in the top panel of figure 6, which also indicates the Curie–Weiss behaviour for $T \geqslant 20.0$ K with $\Theta_c \approx -4.5$ K. The value of Θ_c exactly matches with the value observed for 'free powder' measured at low magnetic field (50.0 Oe). The temperature dependence of ZFC–FC magnetization measured for the 'fixed powder' is shown in the bottom panel of figure 6, where the peak in the ZFC magnetization remains unaltered at $T_f = 18.0$ K. In addition, the values of T_f are found to decrease with increasing H, where the peak at T_f is rounded off at high magnetic field. The H dependence of T_f fits satisfactorily with the Almeida–Thouless (AT) relation as $T_f \propto H^{2/3}$ over a range between 50.0 Oe and 10.0 kOe, which is shown in the inset of the bottom panel of the figure by the continuous straight line [10]. The field dependence of spin freezing temperature following the AT line up to ∼2.8 kOe has also been reported for amorphous Fe_2O_3 [5]. In the low field region the AT line is commonly observed for typical SG compounds [11–13]. On the other hand, the AT line also holds satisfactorily for different systems such as nanoparticles [14] and anisotropic ferromagnets [15]. However, the recent theoretical and experimental results indicate that the field dependence of spin freezing temperature following the AT relation does not confirm the unique feature of SG behaviour [16, 17].

The magnetic hysteresis loop was measured at 5.0 K ($\ll T_f$) for the 'free powder' and 'fixed powder'. We note that the magnetic hysteresis loop including the magnetization at the 50.0 kOe does not repeat for the 'free powder', which changes remarkably for different sets of measurements. On the other hand, the magnetic hysteresis loop at 5.0 K repeats exactly for the 'fixed powder', which is shown in figure 7. The value of coercivity is 1.70 kOe, which is comparable to the coercivity reported by Mukadam *et al* for amorphous Fe_2O_3 [5]. The features of the magnetization curves for the 'free powder' and 'fixed powder' indicate that the particles rotate physically for free powders, which results in the different magnetization curves for 'free powder'. In the case of a small magnetic field with $H = 50.0$ Oe the rotation of the particles is negligible and the value of Θ_c exactly matches with the value obtained for the 'fixed powder', where the particles cannot rotate physically. In the case of a higher applied field for $H > 50$ Oe the magnetic field is sufficient to rotate or align a certain percentage of particles below T_f resulting in the ambiguous results in the temperature and magnetic field dependence. In order to avoid ambiguity we proceed further for the magnetization study with the 'fixed powder'.

It is difficult to explain the blocking process at 10.0 K for the particles with average size ∼85.0 nm. Moreover, the large distribution of particles reveal the typical broadened peak in contrast to the nearly sharp peak at 18.0 K. We note that T_f in the ZFC magnetization following the AT line may indicate the spin freezing temperature. The relaxation of the magnetization was measured for the 'fixed powder' under the following experimental protocol in order to characterize the low temperature state. The sample was cooled down to 10.0 from 100.0 K ($\gg T_f$) in zero magnetic field, left for two different delay times (t_w), and then the magnetization was recorded over time in a 10.0 Oe magnetic field. The time

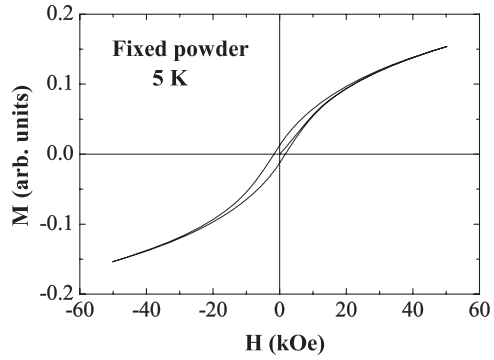

Figure 7. Magnetic hysteresis loop at 5.0 K for the 'fixed powder'.

dependence of magnetization at $t_w = 600$ and 1800 s is shown in the top panel of figure 8. Various functional forms have been proposed to describe the magnetization as a function of t at different t_w. The most popular relation is the stretched exponential, $M(t) = M_g \exp[-(t/\tau)^{1-n}]$, where M_g is the magnetization involved with the glassy magnetic component. M_g and τ (time constant) depend on temperature (T) and t_w, while n is only a function of T. The relaxation involves the activation against a single energy barrier for $n = 0$ and the non-zero value of n ($0 < n < 1$) stands for the distribution of energy barriers commonly observed for SG compounds. Here, the relaxation of magnetization is reproduced well by the stretched exponential, which is indicated by the continuous curves in the top panel of figure 8. Values of $n \approx 0.4$, and $\tau \approx 9000$ and 10 000 s for t_w at 600 and 1800 s, respectively, are observed, indicating the slow increasing trend of τ with t_w. Recently, the spin-cluster state in amorphous Fe_2O_3 has been reported by Mukadam *et al*, where the coexistence of ferromagnetic and glassy magnetic components was reported in the relaxation of dc magnetization [6]. The spin dynamics in amorphous Fe_2O_3–TeO_2 glass was also reported by Akamatsu *et al*, where only a glassy magnetic component in the relaxation of dc magnetization was observed suggesting the prototype spin-glass behaviour at low temperature [7]. Here, we observe only the glassy magnetic component in the relaxation of magnetization. In the case of classical SG compound the t dependence of magnetization exhibits a point of inflection at t_w, and a strong dependence of magnetization against the t plot at different t_w is observed below the SG transition temperature. A crossover from the quasi-equilibrium to the non-equilibrium state is observed around t_w, which is clearly indicated by a peak in the plot of the magnetic viscosity, defined as $S(t) = (1/H)\mathrm{d}M(t)/\mathrm{d}(\ln t)$, against t plot at t_w [18, 19]. The above ageing phenomenon is commonly observed for SG systems, which further indicates the cooperative relaxation process below the spin freezing temperature. The plots of $S(t)$ as a function of t with t_w at 600 and 1800 s are shown in the bottom panel of figure 8. Here, we also observe the peak in the $S(t)$ against t plot at t_w indicating the signature of a cooperating relaxation process analogous to the typical SG compounds.

We investigate the memory effect using a dc magnetization study, which was originally developed to characterize the SG compounds. The sample was cooled down to 2.0 from

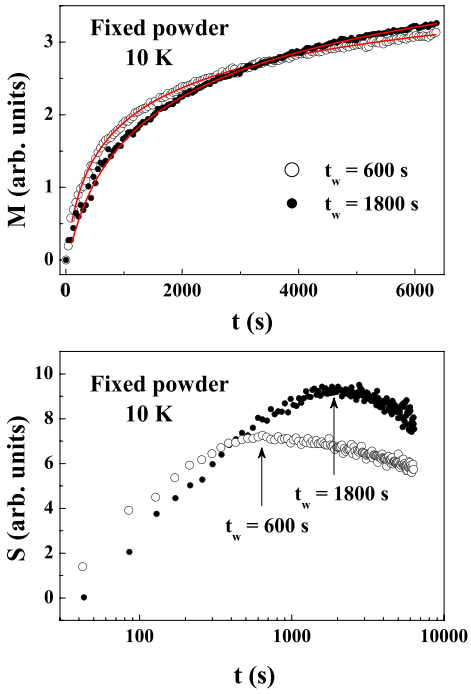

Figure 8. Time (t) dependence of magnetization at two different waiting times (t_w) for the 'fixed powder' where the solid curves show a satisfactory fit using the stretched exponential as described in the text (top panel). Magnetic viscosity against time at different t_w as described in the text. Arrows indicate the time t_w (bottom panel).

26.0 K ($>T_f$) in a 50.0 Oe field and the magnetization was recorded during the cooling process. In the cooling process the sample temperature was fixed at 14 and 8.0 K for 1 h when the field was cut off and the magnetization allowed to relax. The measurement was resumed by applying a 50.0 Oe field at the end of a wait of 1 h. After reaching the base temperature at 2.0 K the sample was warmed continuously and the magnetization was recorded in the same field. As seen in figure 9 steps appear in the cooling magnetization curve at 8.0 and 14.0 K, where the sample temperature was halted for 1 h. Notably the step-like feature is also observed around 8.0 and 14.0 K in the heating cycle, despite the sample being warmed continuously. The memory effect in the temperature dependence of magnetization is analogous to the memory effect found in SG compounds, interacting and noninteracting nanoparticles [20–23]. In case of noninteracting nanoparticles the memory effect was suggested as being due to the broad distribution of particle size or distribution of relaxation times [21–23]. On the other hand, the strong interparticle interaction may result in SG or SG-like behaviour for nanoparticles, which is also responsible for the memory effect [24, 20, 25]. Here, the memory effect may be associated with the SG-like behaviour below T_f.

3.3. Mössbauer results

A Mössbauer study has been performed on the 'free powder' in the absence of an external magnetic field. Since the Mössbauer investigation is performed in zero field, the ambiguity ascribed to the rotation of particles is absent for the 'free powder'.

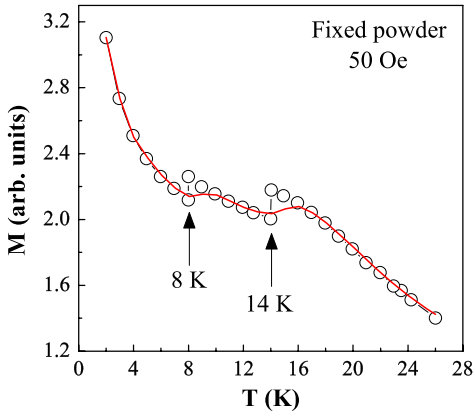

Figure 9. Illustration of the memory effect at 8.0 and 14.0 K in the temperature variation of the field-cooled magnetization for the 'fixed powder' as described in the text.

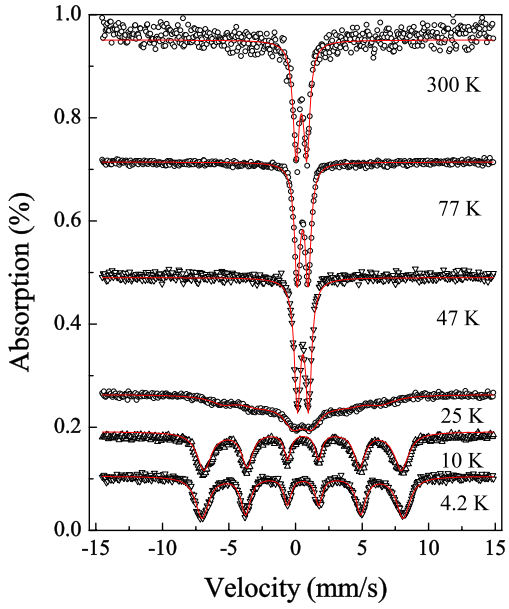

Figure 10. Mössbauer spectra recorded at different temperatures exhibiting different characteristic features. The continuous curves indicate the satisfactory fit of the experimental spectra.

Mössbauer spectra were recorded in the temperature range between 4.2 and 300.0 K. Different characteristics of the spectra with temperature are shown in figure 10. The quadrupole doublet spectrum is observed at 300.0 K. The values of quadrupole splitting in the paramagnetic state are considerably higher than that of the crystalline phase of α/γ-Fe_2O_3. The quadrupole splitting is a measure of the deviation from spherical or cubic symmetry, which appears in the spectrum as a result of the interaction between the quadrupole moment of ^{57}Fe and the local electric field gradient (EFG). The value of quadrupole splitting (QS1) is simplified as QS1 $= eQV_{zz}/2$ for the ^{57}Fe Mössbauer resonance, where e, Q, Z_{zz} are the charge on the proton, magnitude of charge deformation, and principal component of the EFG tensor, respectively. Here, the values of QS1 are found in between 0.8 and 0.91 mm s^{-1} at different temperatures in the paramagnetic state (table 1); this is in the range 0.54–0.91 mm s^{-1} reported for amorphous Fe_2O_3 [26, 9]. The spectra exhibit a paramagnetic quadrupole doublet pattern for $T > 25.0$ K, while the magnetically split sextet pattern is observed for $T \leqslant 25.0$ K consistent with the magnetization results. The signature of the ordering temperature is typically found at higher temperature for Mössbauer investigation than that of the value observed in the magnetization study, which is ascribed to the different timescale of measurements. Mössbauer spectra in the paramagnetic and frozen state are fitted satisfactorily considering the unique hyperfine field, which confirm the absence of another impurity phase. The continuous curves in figure 10 exhibit the satisfactory fit of the experimental spectra and the fitted parameters are given in table 1. The values of isomer shift (IS) and hyperfine field at 4.2 K are estimated as 0.50 mm s^{-1} and 498.0 kOe, respectively. The value of IS is consistent with the value for nanoparticles of α/γ-Fe_2O_3 and amorphous Fe_2O_3, which indicates the signature of high spin Fe^{3+} [26, 9]. The value of the hyperfine field at 4.2 K is much smaller than for bulk α/γ-Fe_2O_3 (∼531.0 kOe for α-Fe_2O_3 and ∼526.0 kOe for γ-Fe_2O_3) [27] and consistent with the other amorphous Fe_2O_3, where the values of hyperfine field are reported in between 455.0 and 501.0 kOe [26, 28, 29]. The values of quadrupole shift (QS2) are 0.085 and 0.086 for 4.2 and 10.0 K, respectively. The line width of the spectrum at 4.2 K is ∼1.2 mm s^{-1}, which is significantly wider than the typical magnetically split spectrum of crystalline α/γ-Fe_2O_3 at 5.0 K [27]. However, the value of the line width is close to the reported values for amorphous Fe_2O_3 [9, 28].

Table 1. Fitted Mössbauer parameters at different temperatures (T): isomer shift (IS); quadrupole splitting (QS1); quadrupole shift (QS2); hyperfine field (H_{hf}).

	Doublet		Sextet		
T (K)	IS (mm s^{-1})	QS1 (mm s^{-1})	IS (mm s^{-1})	QS2 (mm s^{-1})	H_{hf} (kOe)
4.2	—	—	0.50[b]	0.085[c]	498.0[a]
10.0	—	—	0.56[b]	0.086[c]	489.0[a]
25.0	0.50[b]	0.67[c]	0.52[b]	—	367.0[a]
47.0	0.56[b]	0.83[c]	—	—	—
77.0	0.53[b]	0.80[c]	—	—	—
300.0	0.44[b]	0.80[c]	—	—	—

[a]Error = ±0.5 mm s^{-1}.
[b]Error = ±0.01 mm s^{-1}.
[c]Error = ±0.005 mm s^{-1}.

4. Discussions

Mössbauer results clearly indicate that the porous Fe_2O_3 does not correspond to the crystalline phase of either α-Fe_2O_3 or γ-Fe_2O_3, which is rather consistent with an amorphous structure. Here, the average particle size is ∼85.0 nm, which is much higher than that of the average size reported for the amorphous Fe_2O_3 [29, 6]. Note that amorphous structure is typically observed for small particles, where surface disorder dominates over core crystallinity. The amorphous structure of porous Fe_2O_3 might be ascribed to the porous structure with wall

thickness $<\sim$5.0 nm. In addition, the amorphous structure of the porous oxides is commonly observed in different cases synthesized by the classical surfactant templating method [3, 4]. Recently, the extensive investigations on the static and dynamic aspects of dc magnetization and ac susceptibility measurements suggest a spin-cluster freezing process at low temperature in amorphous Fe_2O_3, where coexistence of ferromagnetic and glassy magnetic components is observed in the relaxation of magnetization [5, 6]. Note that a dipole interaction leading to the spin-glass like behaviour has been observed for magnetic nanoparticles [24, 25, 30, 31], where the dipole–dipole interaction is strong for the amorphous Fe_2O_3 reported by Mukadam *et al* exhibiting a spin-cluster freezing process at low temperature. Akamatsu *et al* have reported typical spin-glass behaviour in the Fe_2O_3–TeO_2 glass, where the critical slowing down behaviour was observed in the frequency dependence of the freezing temperature, memory, and ageing effect in the relaxation dynamics [7]. In case of Fe_2O_3–TeO_2 glass the molar fractions of Fe_2O_3 and TeO_2 were 20% and 80%, respectively, where Fe_2O_3 is diluted by the TeO_2 giving rise to the weak dipole–dipole interaction. The amorphous structure of the materials with antiferromagnetic interactions may lead to a spin-glass like behaviour depending on the degrees of disorder and frustration. Here, we observe that the peak in the ZFC magnetization at T_f does not change between the 'free powder' and 'fixed powder', whereas the dipole–dipole interaction is weakened for the 'fixed powder', because the powdered sample ('free powder') is diluted and fixed in a nonmagnetic stycast to get the 'fixed powder'. An amorphous structure with an antiferromagnetic interaction might be responsible for the spin-glass like behaviour in the present compound, analogous to the Fe_2O_3–TeO_2 glass. However, the existence of pores in the present compound increases the surface to volume ratio significantly, which makes this system unique amongst the reported systems of amorphous Fe_2O_3. In the case of a large surface area the surface magnetism of the compound may dominate the bulk magnetism. The surface effect essentially results from the lack of translational symmetry at the boundaries with lower coordination number and the broken magnetic exchange bonds. It may also be responsible for the spin disorder or random spin canting associated with the occurrence of spin frustration giving rise to spin-glass like behaviour.

In conclusion, the dominant surface effect is observed for the amorphous Fe_2O_3, where the surface to volume ratio is increased by the nanoporous structure. The large magnetic anisotropy is observed for the porous and amorphous Fe_2O_3, where the large anisotropy is attributed to the significant contribution from the surface effect. In the temperature dependence of zero-field cooled magnetization the spin freezing temperature is observed at 18.0 K, where the memory effect in the field-cooled magnetization and the relaxation of magnetization below the spin freezing temperature display similar characteristic features to typical spin-glass systems.

Acknowledgments

This work is supported by DST (Project No. SR/S2/CMP-46/2003) and CSIR (Project No. 03/999/04/EMR-II), India. One of the authors (SG) wishes to thank JSPS, Japan, for the support of a Fellowship for a Foreign Researcher. We would like to thank Mr S Mukhopadhyay for helping us to fit the Mössbauer spectra.

References

[1] Halder G J, Kepert C J, Moubaraki B, Murray K S and Cashion J D 2002 *Science* **298** 1762
[2] Kaneyoshi T 1991 *J. Phys.: Condens. Matter* **3** 4497
[3] Bhaumik A and Inagaki S 2001 *J. Am. Chem. Soc.* **123** 691
[4] Chandra D, Yokoi T, Tatsumi T and Bhaumik A 2007 *Chem. Mater.* **19** 5347
[5] Mukadam M D, Yusuf S M, Sharma P and Kulshreshth S K 2004 *J. Magn. Magn. Mater.* **269** 317
[6] Mukadam M, D, Yusuf S M, Sharma P, Kulshreshtha S K and Dey G K 2005 *Phys. Rev.* B **72** 174408
[7] Akamatsu H, Tanaka K, Fujita K and Murai S 2006 *Phys. Rev.* B **74** 012411
[8] Amores J M G, Escribano V S and Busca G 1999 *J. Mater. Chem.* **9** 1161
[9] van Diepen A M and Th Popma J A 1978 *Solid State Commun.* **27** 121
[10] de Almeida J R L and Thouless D J 1978 *J. Phys. A: Math. Gen.* **11** 983
[11] Kenning G G, Chu D and Orbach R 1991 *Phys. Rev. Lett.* **66** 2923
[12] Chamberlin R V, Hardiman M, Turkevich L A and Orbach R 1982 *Phys. Rev.* B **25** 6720
[13] Petit D, Fruchter L and Campbell I A 1999 *Phys. Rev. Lett.* **83** 5130
[14] Fiorani D, Tholence J and Dormann J L 1986 *J. Phys. C: Solid State Phys.* **19** 5495
Dormann J L, Bessais L and Fiorani D 1988 *J. Phys. C: Solid State Phys.* **21** 2015
[15] Fischer K H and Zippelius A 1987 *Phys. Rev.* B **35** 7171
[16] Katzgraber H G and Young A P 2005 *Phys. Rev.* B **72** 184416
[17] Sahoo S, Petracic O, Ch Binek, Kleemann W, Sousa J B, Cardoso S and Freitas P P 2002 *Phys. Rev.* B **65** 134406
[18] Mydosh J A 1993 *Spin Glasses* (London: Taylor and Francis)
[19] Binder K and Young A P 1977 *Rev. Mod. Phys.* **49** 435
[20] Sun Y, Salamon M B, Garnier K and Averback R S 2003 *Phys. Rev. Lett.* **91** 167206
[21] Sasaki M, Jonsson P E, Takayama H and Nordblad P 2004 *Phys. Rev. Lett.* **93** 139701
[22] Chakraverty S, Bandyopadhyay M, Chatterjee S, Dattagupta S, Frydman A, Sengupta S and Sreeram P A 2005 *Phys. Rev.* B **71** 054401
[23] Tsoi G M, Wenger L E, Senaratne U, Tackett R J, Buc E C, Naik R, Vaishnava P P and Naik V 2005 *Phys. Rev.* B **72** 014445
[24] Thakur M, De K, Giri S, Si S, Kotal A and Mandal T K 2006 *J. Phys.: Condens. Matter* **18** 9093
[25] Thakur M, Chowdhury M, Majumdar S and Giri S 2008 *Nanotechnology* **19** 045706
[26] Murad E and Schwertmann U 1980 *Am. Mineral.* **65** 1044 references therein
[27] Murad E 1988 *Iron in Solids and Clay Minerals* ed J W Stuki, B A Goodman and U Schwertmann (Dordrecht: Reidel) p 309
[28] Ayyub P, Multani M, Barma M, Palkar V R and Vijayraghavan R 1988 *J. Phys. C: Solid State Phys.* **21** 2229
[29] Carpenter E E, Long J W, Rolison D R, Logan M S, Pettigrew K, Stroud R M, Theil Kuhn L, Rosendahl Hansen B and Mrup S 2006 *J. Appl. Phys.* **99** 08N711
[30] Jonsson T, Svedlindh P and Hansen M F 1998 *Phys. Rev. Lett.* **81** 3976
[31] Poddar P, Telem-Shafir T, Fried T and Markovich G 2002 *Phys. Rev.* B **66** 060403(R)